Int. J. Heat Mass Transfer. Vol. 30, No. 9, pp. 1803–1812, 1987
Printed in Great Britain

0017-9310/87 $3.00+0.00

Combined wall-to-fluidized bed heat transfer. Bubbles and emulsion contributions at high temperature

G. FLAMANT and T. MENIGAULT
Institut de Science et de génie des matériaux et procédés, CNRS, BP 5, 66120 Odeillo, France

(*Received* 7 *May* 1986 *and in final form* 21 *November* 1986)

Abstract—A theoretical and experimental investigation of combined wall-to-fluidized bed heat transfer is presented. Bubble and emulsion contributions are modelled assuming both phases to be semi-transparent grey media. For a radiant bubble phase component the general situation of absorbing gases including particulate is described. Tests were performed with a two-dimensional fluidized bed column in the temperature range 500–900°C. Experimental and theoretical results emphasized that (i) a non-linear relation exists between h and T_b if the conduction-to-radiation parameter (N) is smaller than 5, indicating that radiative and conductive contributions are not independent, (ii) the dense phase radiant contribution becomes significant at temperatures higher than 700°C, (iii) at 900°C the bubble phase radiative component cannot be neglected.

INTRODUCTION

FOR OPERATIONS in high-temperature fluidized beds such as combustion, the potential contribution of thermal radiation to heat transfer is an important design parameter. A detailed analysis of the literature dealing with heat transfer between a fluidized bed and immersed surfaces at about 900°C has been done by Flamant and Arnaud [1]. Previous studies collectively suffer the limitations given below.

(1) Most of the investigations conclude that the radiative contribution is significant but conflicting predictions remain on the importance of the radiative component: the evaluation ranges from 15 to 50% for a 900°C bed temperature [2–12].

(2) The bubble phase radiative contribution, h_{Br}, is neglected except by Yoshida *et al.* [13]. Nevertheless they conclude that h_{Br} is negligible ($<5\%$) up to 1300°C.

(3) Previous models are based on simple assumptions such as: the heat transfer components are independent (radiation–conduction interaction is neglected); the gas is assumed to be transparent and radiative transfer is described as a heat exchange between black (Vedamurthy and Sastri [11]), or grey (Kolar *et al.* [8]), opaque surfaces. In addition no satisfying interpretation of the h vs T_b relation was proposed.

(4) Different methods have been proposed for the measurement of the overall or radiant heat exchange coefficient: transparent wall (Szekely and Fisher [14]), cylindrical (Jolley [7]) or spherical (Kharchenko and Makhorin [15]) calorimeters, radiometer probes (Il'chenko *et al.* [5], Vadivel and Vedamurthy [16], Ozkaynak *et al.* [17]). But all these devices concern local measurements of the heat transfer coefficient whereas mean values are generally more useful for design applications.

In order to take into account the radiative transport phenomena in such a particulate system—the radiant intensity is attenuated by absorption and scattering and is increased by emission—we introduce the conceptual model developed to describe the heat exchange through semi-transparent media. The dense phase is considered to be an optically thick medium and we assume that bubbles are composed of absorbing gases (H_2O, CO_2) including particulate. The experimental study is performed using a two-dimensional stainless steel column heated by infra-red heaters. A correlation of experimental data in the bed temperature range 500–900°C for alumina and silicon carbide particles (280–1000 μm) is proposed. Finally the comparison between experimental and theoretical results is presented.

THEORETICAL

In high temperature gas–solid fluidized media the heat is exchanged between immersed surfaces and the bed by conduction–radiation and convection in the emulsion phase and by radiation through the bubbles. The overall heat transfer coefficient may be written as

$$h_t = (1-f_0)(h_{et}+h_{ec})+f_0 h_{Br} \qquad (1)$$

where f_0 is the fraction of heat transfer surface area exposed to bubbles, h_{et} and h_{ec} the conduction–radiation and convection emulsion contributions, respectively, and h_{Br} the radiant bubble phase contribution.

The variations of components h_{et} and h_{Br} are analysed below.

NOMENCLATURE

Ar	Archimede number, $gd^3\rho_g(\rho_p-\rho_g)/\mu^2$
B	coefficient in equation (23)
C	specific heat [J kg^{-1} °C^{-1}]
C_s	correction factor in equation (18)
d, D	diameter [m or μm]
f_B	bubble frequency [s^{-1}]
f_0	fraction of heat transfer surface exposed to bubbles
f_v	volumetric fraction of particles
F	view factor between wall and emulsion, $(1/\varepsilon_e+1/\varepsilon_w-1)^{-1}$
F_g	gas mass flow rate [kg s^{-1}]
h	heat transfer coefficient [W m^{-2} °C^{-1}]
J	radiosity [W m^{-2}]
k	absorption index
K	extinction coefficient of the emulsion, $\kappa+\sigma_s$ [m^{-1}]
L_v	Spectral intensity [W m^{-2} sr^{-1}]
n_c	complex refractive index, $n(1+ik)$
N	conduction-to-radiation interaction parameter, $\lambda_e K/4\sigma T_b^3$
Nu	Nusselt number, $h_t d/\lambda_g$
p_i	pressure of component i
P	heat losses in equation (28) [W]
q	flux density [W m^{-2}]
Q_a, Q_s	single particle absorption and scattering efficiency, respectively
R	mean path length [m]
R_c	heat transfer resistance, δ_g/λ_g [m^2 °C W^{-1}]
t	time [s]
t^*	non-dimensional time, $(\lambda_e/\rho_e C_e)/K^2 t$
t_r	residence time of the packet
S	heat transfer area between wall and fluidized bed [m^2]
T	temperature [K]
T'	rear wall temperature [K]
U, U_{mf}	fluidization and minimum fluidization velocities, respectively [m s^{-1}]
V	volume [m^3].

Greek symbols

α	$4/3N$
β	$(4R_c F\sigma T_b^3)^{-1}$
δ_{ij}	Kroneker symbol
γ	N/F
δ_g	gas film thickness
ε	total hemispherical emissivity
ε_s	particulate emissivity
θ	dimensionless temperature, T/T_b
θ_s	emulsion surface dimensionless temperature
λ	thermal conductivity [W m^{-1} °C^{-1}]
μ	dynamic viscosity
κ	absorption coefficient [m^{-1}]
ω_s	albedo
ρ	density [kg m^{-3}]
σ	Stefan–Boltzmann constant
σ_s	scattering coefficient [m^{-1}]
τ	non-dimensional space coordinate, Kx
τ_B	optical depth
τ_{ij}	gas transmissivity between surfaces i and j
ϕ	net flux density on the transfer wall [W m^{-2}]
ϕ^+	dimensionless flux, $\phi/4F\sigma T_b^3$

Subscripts

b	fluidized bed
B	bubble
c	conductive, convective
e	emulsion
g	gas
i	internal
i	instantaneous
p	particle
r	radiative
t	total
w	wall
v	spectral.

Superscripts

i	inlet
′	rear wall.

Emulsion phase component

Let us summarize the model previously detailed in ref. [1]. Based on the 'packet model', conduction and radiation wall-to-emulsion heat exchanges are described as combined phenomena. The dense phase is assumed to be an optically thick semi-transparent semi-infinite grey medium bounded by a film near the wall. The radiative properties of the packet are : ε_e and K, emissivity and extinction coefficient, respectively. During the residence time of the packet (t_r) the heat is exchanged by conduction and radiation. The energy equation can be written as

$$\rho_e c_e \frac{\partial T}{\partial t} + \nabla(q_c + q_r) = 0. \quad (2)$$

For a one-dimensional optically thick semi-infinite grey medium the radiative flux is defined as (Rosseland approximation)

$$q_r = -\frac{16n^2\sigma T^3}{3K}\frac{\partial T}{\partial x}. \quad (3)$$

By introducing the conduction-to-radiation interaction parameter N (Planck number), the dimen-

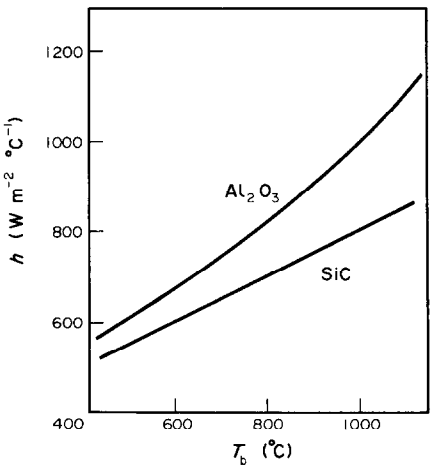

FIG. 1. Theoretical results. Heat transfer coefficient vs bed temperature: $d = 0.3 \times 10^{-3}$ m, $\delta_g = d/6$. SiC, $K = 5000\,\mathrm{m}^{-1}$; Al_2O_3, $K = 500\,\mathrm{m}^{-1}$.

sionless form of equation (2) is

$$\frac{\partial\theta}{\partial t^*} = \frac{\partial}{\partial\tau}\left[\left(1+\frac{4}{3N}\theta^3\right)\frac{\partial\theta}{\partial\tau}\right]. \quad (4)$$

The previous equation is solved numerically according to the following boundary conditions:

$$-t^* = 0 \quad \tau > 0 \quad \theta(\tau, t^*) = 1 \quad (5)$$

$$-\tau \to \infty \quad t^* > 0 \quad \theta(\tau, t^*) = 1. \quad (6)$$

When $\tau = 0$ a constant flux density at the boundaries: wall–gas film and gas film–emulsion is assumed, then it becomes

$$\phi^+ = \beta + \tfrac{1}{4}(\theta_w+\theta_s)(\theta_w^2+\theta_s^2)(\theta_w-\theta_s)$$

$$\phi^+ = \gamma(1+\alpha\theta_s^3)\left.\frac{d\theta}{d\tau}\right|_{\tau=\tau_g}. \quad (7)$$

The instantaneous heat transfer coefficient is then expressed as

$$h_i^+ = \frac{\phi^+}{\theta_w - 1}.$$

Theoretical results indicate that at a temperature higher than 700°C the heat transfer coefficient vs bed temperature profiles are nonlinear when $N < 5$, i.e. when conduction and radiation are combined. On the contrary, as shown in Fig. 1, when $N > 5$ the emulsion may be considered as an opaque medium: the thermal radiation is exchanged between the wall and the packet adjacent surface and the heat is transferred only by conduction through the packet.

Bubble phase radiative component

For application such as combustion, the bubbles are composed of absorbing gas in the infra-red spectrum: CO_2 and H_2O. In addition a small amount of particles may be present in bubbles, the volumetric fraction of solids, f_v, ranging from 10^{-3} to 10^{-2} [18].

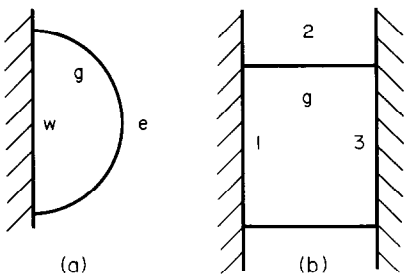

FIG. 2. Physical model for bubble radiative heat transfer.

We have taken into account either small particles such as soot ($d < 1$ μm) or large particles such as carbon fines for example.

A simplified physical representation of a bubble is adopted: half a sphere in a three-dimensional bed and a cylinder in a two-dimensional column as shown in Fig. 2. The radiative transfer between wall and bubble, filled with gas and bounded by emulsion, is governed by the equation of net radiation, Siegel and Howell [19] describing the exchange in a grey enclosure containing an isothermal gas. The main assumptions are:

(a) the temperature is uniform;

(b) the surface radiative properties are independent of wavelength and direction, so that: $\varepsilon_j = \alpha_j = 1-\rho_j$;

(c) all energy is emitted and reflected diffusely.

Introducing J_j the radiosity of surface j (rate of outgoing radiant energy per unit area), F_{ij} the view factor between surfaces i and j, τ_{ij} the transmissivity of the gas at T_g for the thermal radiation at T_i, q_i and ε_i the net flux density lost by i and its emissivity; the heat balance equations are

$$\sum_{j=1}^{n}[\delta_{ij}-(1-\varepsilon_i)F_{ij}\tau_{ij}]J_j = \varepsilon_i\sigma T_i^4 + (1-\varepsilon_i)\varepsilon_g\sigma T_g^4 \quad (8)$$

and

$$q_i = \frac{\varepsilon_i}{1-\varepsilon_i}(\sigma T_i^4 - J_i). \quad (9)$$

For semi-spherical and cylindrical bubbles the number of surfaces n is equal to two and three, respectively. In the first case, if the gas is transparent note that equations (8) and (9) reduce to

$$q_w = \frac{2\sigma(T_w^4 - T_b^4)}{\dfrac{2}{\varepsilon_w}+\dfrac{1}{\varepsilon_e}-1}. \quad (10)$$

This equation was proposed by Yoshida *et al.* [13] to calculate the radiant heat transfer component in fluidized beds.

To solve the general problem, the gas emissivity, ε_g, and the gas transmissivity, τ_{ij}, must be calculated assuming the following relation between transmissivity and absorptivity:

$$\tau_{ij} = 1-\alpha_{ij}. \quad (11)$$

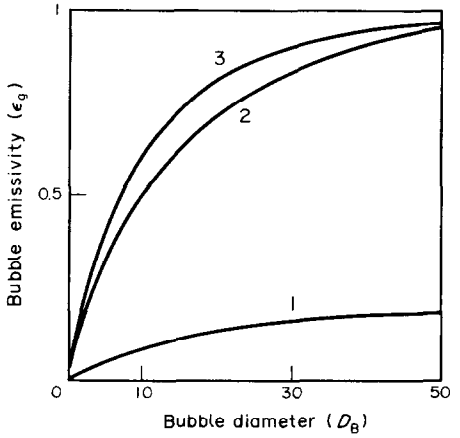

FIG. 3. Gas emissivity vs bubble diameter: 1, CO_2–H_2O mixture, $p_{H_2O} = 0.14$, $T_g = 800°C$, $p_t = 1$ atm; 2, carbon fines in CO_2, $d = 10$ μm, $f_v = 10^{-3}$, $T_g = 800°C$, $P_t = 10$ atm, $p_{CO_2} = 1$ atm; 3, soot in CO_2, $d = 0.1$ μm, $f_v = 10^{-5}$, $T_g = 800°C$, $p_t = p_{CO_2} = 1$ atm.

In the previous equation α_{ij} is the gas absorptivity at temperature T_g for the black body radiation at T_i and for the mean length R_{ij}

$$\alpha_{ij} = \alpha_{ij}(T_g, T_i, R_{ij}). \tag{12}$$

For example, ε_g and α_{ij} are related, for steam, by

$$\alpha_{ij} = \left[\frac{T_g}{T_i}\right]^{0.45} \varepsilon_g. \tag{13}$$

Generally a rough approximation is obtained assuming $\alpha_{ij} = \varepsilon_g$.

Some examples will now be given to illustrate the bubble emissivity as a function of composition and radius.

Bubble emissivity

The bubble spectral emissivity can be expressed as

$$\varepsilon_{vg} = 1 - \exp(-\kappa_v R_B) \tag{14}$$

in which κ_v is the spectral absorption coefficient and R_B the path length. R_B may be approximated by

$$R_B = 0.9 \times 4 \times \frac{V_B}{S_B} \tag{15}$$

where V_B and S_B are the volume and the surface of the bubble. The total emissivity is then given by

$$\varepsilon_g(T_g) = \frac{\pi \int_0^\infty [1 - \exp(-K_v R_B)] L_v^0(T_g)\, dv}{\sigma T_g^4} \tag{16}$$

where $L_v^0(T_g)$ is the black body intensity at T_g.

For H_2O and CO_2 without particulate we used the data of Hottel and Sarofim's band model [20] to calculate curve 1 in Fig. 3, which is representative of bubbles in a fluidized bed calciner.

To account for isotropically scattering particulate in a CO_2 bubble, Skocypec and Buckius' [21] study is very useful. The expression of total emissivity is

$$\varepsilon_g = \varepsilon_s + C_s \varepsilon_{CO_2} \tag{17}$$

where ε_s is the emissivity of the particulate medium containing no gaseous absorption and ε_{CO_2} the gas emissivity without scattering particulate. C_s is a correction factor function of temperature T_g, p_{CO_2}, R_B, albedo $\omega_s = \sigma_s/(\kappa+\sigma_s)$ and optical depth $\tau_B = (\kappa+\sigma_s)R_B$. C_s is tabulated vs $(1-\omega_s)\tau_B$ in ref. [21].

Theoretical predictions are related to carbon fines ($d > 1$ μm) and soot ($d < 1$ μm).

Carbon fines ($d = 10$ μm). According to ref. [20], the particulate emissivity can be written as

$$\varepsilon_s = 1 - \exp\left[-1.5 f_v \frac{R_B}{d}\right] \tag{18}$$

in which f_v is the volumetric fraction of solid.

To evaluate the correction factor C_s, albedo and optical depth must be calculated. Assuming monodispersion of spherical particles, Brewster and Tien [22] proposed

$$\sigma_s = 1.5 Q_s \frac{f_v}{d}$$
$$\kappa = 1.5 Q_a \frac{f_v}{d} \tag{19}$$

where Q_s and Q_a are the single scattering and absorption efficiencies, for opaque spheres

$$Q_s = 1 - \varepsilon_s$$
$$Q_a = \varepsilon_s. \tag{20}$$

Then τ and ω_s can be expressed as

$$\tau = 1.5 f_v \frac{R_B}{d}$$
$$\omega_s = 1 - \exp\left(-1.5 f_v \frac{R_B}{d}\right). \tag{21}$$

Curve 2 on Fig. 3 gives the relation between ε_g and D_B for $f_v = 10^{-3}$. Note that the bubble emissivity is large even for small diameters: e.g. $\varepsilon_g = 0.5$ for $D_B = 10^{-2}$ m.

Soot ($d = 0.1$ μm). Particulate emissivity can be expressed as [23]

$$\varepsilon_s = 1 - \frac{15}{\pi^4} \psi^{(3)} \left[1 - \frac{B f_v R_B T_g}{C_2}\right] \tag{22}$$

in which

$$\psi^{(3)}(z) = \int_0^\infty \frac{t^3 \exp(-zt)}{1 - \exp(-t)} dt,$$
$$C_2 = 1.44 \times 10^{-2} \text{ m K} \tag{23}$$

and

$$B = \frac{36\pi n^2 k}{[n^2(1-k^2)+2]^2 + 4n^2k^2}$$

where n and k are the optical constants of soot, with $n_c = n(1+ik)$ the complex refractive index of the particles.

In addition κ and σ_s are defined as

$$\left.\begin{aligned}\kappa &= B\frac{f_v}{\lambda}\\ \sigma_s &= 1.5 f_v \frac{Q_s}{d}\end{aligned}\right\} \qquad (24)$$

which according to ref. [24]

$$Q_s = 2+0.5\left[\frac{\pi d}{\lambda}\right]^{-8/9}.$$

The parameters n, k, κ, and σ_s, depend on the chemical composition of soot, and wavelength. To evaluate mean values of these parameters, the optical constants are calculated at $\lambda = 2.5$ μm, corresponding roughly to the maximum black body emission at $T = 1100$ K. According to ref. [25] the complex refractive index is equal to

$$n_c = 2.04 - i\,1.15 \qquad (25)$$

for a ratio H/C = 1/4.6 and $\lambda = 2.5$ μm.

Equations (25), (24), (23) and (22) are used to calculate the ε_g vs D_B profile shown as curve 3 on Fig. 3.

Net flux density exchange between wall and bubble

The wall-to-bubble radiant exchange flux depends on the temperatures T_w, T_e, T_b, T_g and on the emissivities ε_w, ε_e and ε_g. Figures 4 and 5 illustrate the $q_{w,B}$ vs ε_g profiles for $T_g = T_b$ and $T_g \neq T_b$. In the first case the radiant flux exchange between wall and bubble increases with bubble emissivity. On the contrary when $T_g = (T_b + T_w)/2$ (Fig. 4) the exchange flux decreases when ε_g increases for an emulsion emissivity larger than 0.3. There exists a maximum of $q_{w,B}$ for ε_g ranging from 0.1 to 0.5 for the 2-D column (Fig. 5).

Note that for a given value of ε_g, the absolute intensity of radiant heat exchange does not depend on the temperature gradient $T_w > T_e$ or $T_w < T_e$ (for given temperature values).

On Fig. 6 the net flux variations are plotted vs bubble diameter for a three-dimensional column. The corresponding bubble radiant component is expressed as

$$f_0 h_{Br} = f_0 \frac{q_{w,B}}{T_w - T_b}. \qquad (26)$$

For $f_0 = 0.3$, typical values of $f_0 h_{Br}$ range from 40 to 80 W m^{-2} °C^{-1} when $T_w = 900$°C and $T_b = 800$°C (or $T_b = 900$°C and $T_w = 800$°C).

In conclusion we have shown that the bubble radiant heat exchange component is very sensitive to the bubble gas composition. If bubbles contain an absorbent gas and (or) particulates the wall-to-bubble radiant flux can be twice as great or small than when transparent gas is considered. Theoretical results indicate that h_{Br} is significant for bed temperatures over 800°C.

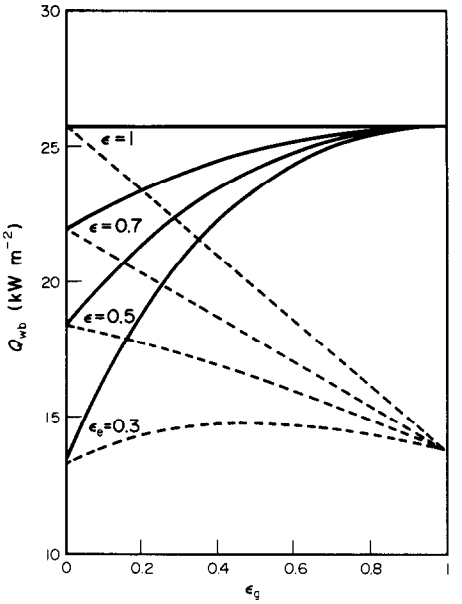

FIG. 4. Wall-to-bubble radiative heat flux vs bubble gas and emulsion emissivities, $\varepsilon_w = 0.8$—three-dimensional column: (a) continuous lines, $T_w = 900$°C, $T_g = T_e = T_b = 800$°C; (b) dashed curves, $T_w = 900$°C, $T_g = 850$°C, $T_e = T_b = 800$°C.

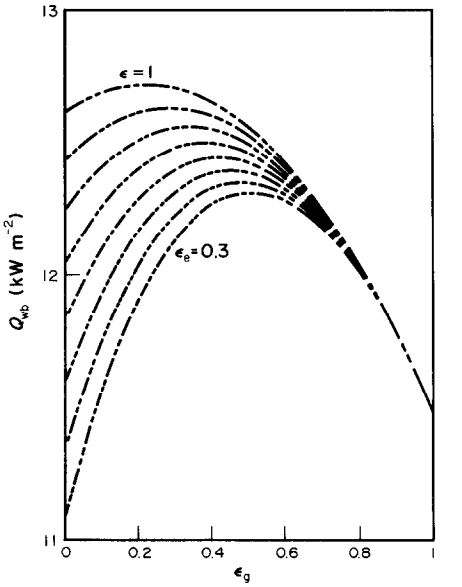

FIG. 5. Wall-to-bubble radiative heat flux vs gas and emulsion emissivities in a two-dimensional column (bed thickness 2 cm): $D_B = 10^{-2}$ m, $\varepsilon_w = 0.6$, $T_{w1} = 900$°C, $T_{w2} = T_b = 800$°C $= T_g$, $T_{w3} = 750$°C.

To compare the predicted overall heat exchange coefficient and experimental values, a large experimental set-up was developed.

EXPERIMENTAL

Experimental system and method

The experimental set-up is shown in Fig. 7 and detailed in ref. [26]. The two-dimensional column is

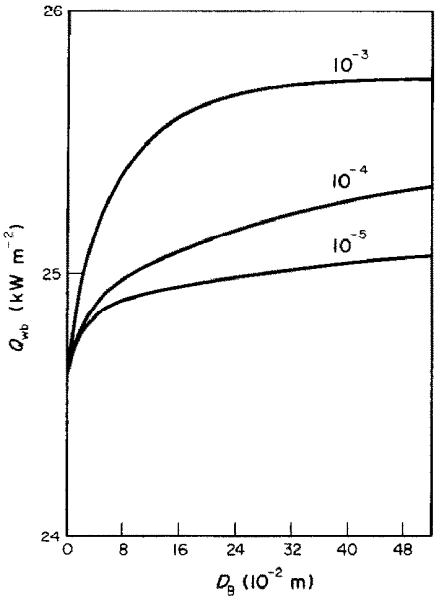

FIG. 6. Wall-to-bubble radiative heat flux vs bubble diameter and volume fraction of solid (carbon fines $d = 10$ μm)—three-dimensional column.

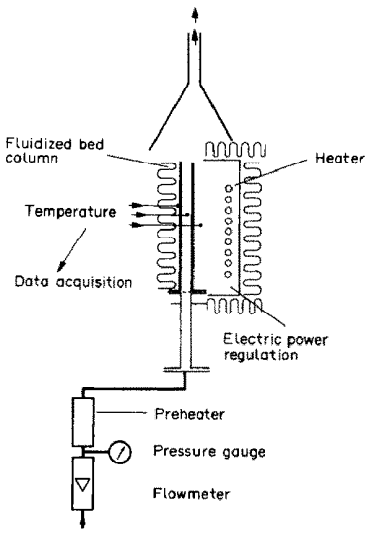

FIG. 7. Experimental set-up.

composed of two parallel refractory stainless steel plates the dimensions of which are: height, 0.75 m; width, 0.49 m; thickness, 0.02 m. The fluidized bed thickness is 25×10^{-3} m. The transfer wall is placed in front of an infra-red heater composed of nine silicon carbide electric resistances mounted before a ceramic wall, the heating area is 0.4 m^2. A power regulation permits operations between 5 and 40 kW, thus a flux density up to 100 kW m^{-2} can be reached on the front wall. The column rear wall is insulated with a 0.15 m alumina layer.

The temperature distributions inside the bed, on the front wall and on the back wall of the column are measured by means of 56 bare or welded thermocouples. In order to calculate the net flux density absorbed by the bed, the heat balance over the whole device is set by measuring the air mass flow rate, the electric power and mean, wall, bed and ambient temperatures. At steady state the heat balance over the fluidized column may be written as

$$\begin{bmatrix}\text{heat exchange}\\ \text{between the wall}\\ \text{and the bed}\end{bmatrix} = \begin{bmatrix}\text{gas enthalpy}\\ \text{increase}\end{bmatrix} + \begin{bmatrix}\text{heat exchange}\\ \text{between the bed}\\ \text{and the rear wall}\end{bmatrix} + [\text{losses}]$$

$$h_t S(T_{wi} - T_b) = F_g C_g (T_b - T_g^i) + h_t' S(T_b - T_{wi}') + P. \tag{27}$$

Neglecting P and the difference between the front and rear wall-to-bed heat transfer coefficients ($h_t = h_t'$), equation (27) can be simplified as

$$h_t = \frac{F_g C_g (T_b - T_g)}{T_{wi} - T_{wi}' - 2T_b}. \tag{28}$$

Equation (28) is related to mean values of T_b, T_w, T_w' and h_t.

The experimental parameters are: bed temperature, air velocity (ratio U/U_{mf}), particle diameter. In order to point out the significance of radiative properties of particles on heat transfer, alumina and silicon carbide particles were selected. The range of experimental parameters is summarized in Table 1.

Results

The data are related to maximum values of the heat transfer coefficient.

Typical h_t vs T_b curves are plotted on Fig. 8 for 280 μm Al_2O_3 and SiC particles. For alumina, the increase of h_t vs T_b is nonlinear at a temperature greater than 700°C and reaches 60% when the bed temperature rises from 500 to 900°C. For silicon carbide a linear relationship is observed and a 40% increase is noted in the same temperature range. The same trend is measured for all particle diameters as shown on the same figure.

A h_t vs d plot is shown in Fig. 9 for alumina particles. Note that the difference between isotherms increases with particle diameter. This result is consistent with the conclusion of Vadivel and Vedamurthy [16]: the radiative contribution rises with particle diameter. An interpretation of this observation is introduced next according to the previous model.

DISCUSSION

The measured heat transfer coefficients exhibit the expected dependence on N, i.e. on temperature and extinction coefficient (see Fig. 1). To compare experimental and theoretical results five parameters must be known: fraction of surface area exposed to bubble

Table 1. Experimental parameters

Material	Al_2O_3	SiC
Diameter (10^{-6} m)	280, 425, 600, 1000	280, 600
Bed temperature (°C)	500–900	
Air mass flow rate (10^{-3} kg s^{-1})	3–30	
Fluidization number (U/U_{mf})	1.5–5	
Net flux density (kW m^{-2})	20–70	

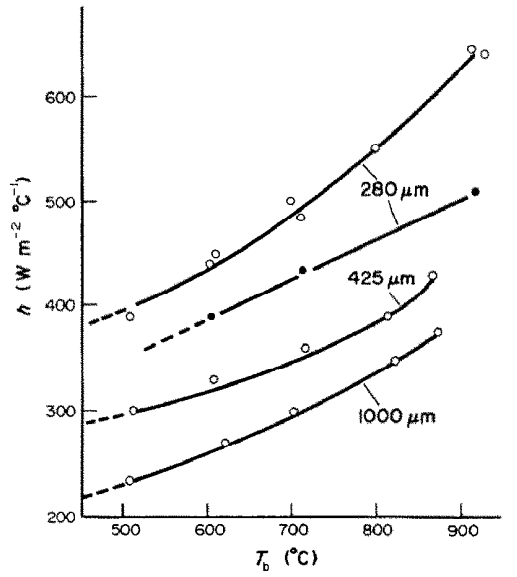

FIG. 8. Experimental results. Overall maximum heat transfer coefficient vs bed temperature: ○, alumina; ●, silicon carbide.

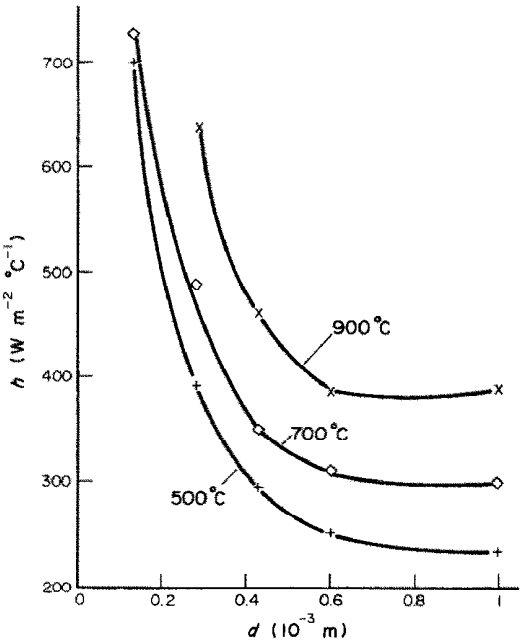

FIG. 9. Experimental results. Overall maximum heat transfer coefficient vs particle diameter and temperature for Al_2O_3 beds.

(f_0), bubble diameter (D_B), residence time of the packet (t_r), gas film thickness (δ_g) and extinction coefficient (K).

The fractional surface f_0 and bubble diameter are evaluated according to Granier's experimental data [27] related to low temperature heat transfer measurements in a two-dimensional fluidized bed column.

The mean residence time of the packet at the wall is obtained from

$$t_r = \frac{1-f_0}{f_B}. \quad (29)$$

in which f_B is the bubble frequency. The variation of f_B with U/U_{mf} and T_B was measured by recording the temperature fluctuations at the surface of the wall [26].

Finally two undetermined parameters remain: δ_g and K. A first numerical estimation of h_{et} is realized as a function of δ_g, then the value of K is fitted by comparison between experimental and theoretical data, taking into account the bubble radiative and the convective contributions. The value of $\delta_g = d/3$ gives coherent results in all cases.

h_{Br} is calculated according to the previous model for cylindrical bubbles of 10 cm mean diameter and transparent gas.

In order to estimate the convective component, the correlation of Botterill and Denloye [28] is selected

$$\frac{h_{ec}d^{1/2}}{\lambda_g} = 0.86Ar^{0.39}, \quad 10^3 < Ar < 10^6. \quad (30)$$

A comparison between experimental and theoretical heat transfer coefficients is shown in Table 2.

The mean deviation between theoretical and experimental values is about 5% in the range 500–900°C and the maximum deviation is less than 10% assuming a constant value for the extinction coefficient (K).

Table 2 shows that the conduction-to-radiation parameter N is less than 5 for alumina particles suggesting that radiative transfer influences the transient temperature profile through the emulsion and consequently the heat transfer coefficient. The non-linear variation of h vs T in this situation is related to the relation $N < 5$ as shown by the theoretical study [1]. For silicon carbide particles, $N > 5$, conduction is the dominant transfer mode and radiant exchange is limited at the boundary wall–emulsion.

In addition, the calculated K values listed in Table 2 are consistent with the measured values from ref. [29]: for Al_2O_3: $500 < K < 1000$ m^{-1} and for SiC: $K = 5000$ m^{-1}.

At 900°C, it can be concluded from the data of Table 2 that the radiative contribution is significant because the ratio h_{Br}/h_t ranges from 5 to 9%. Note

Table 2. Comparison between experimental and theoretical overall heat transfer coefficient $\delta_g = d/3$, $\varepsilon_e(Al_2O_3) = 0.6$, $\varepsilon_e(SiC) = 0.95$

Material	Al_2O_3		Al_2O_3		SiC	
$d(\mu m)$	280		1000		600	
T_b (°C)	504	900	507	872	519	896
$h_{t,exp}$ (W m^{-2} °C^{-1})	390	640	235	375	280	405
K (m^{-1})†	1000	1000	500	500	5000	5000
N	1.86	0.74	0.92	0.39	25	9.3
t_r (s)	0.42	0.37	0.45	0.40	0.44	0.37
$(1-f_0)h_{et}$ (W m^{-2} °C^{-1})	336	568	176	279	231	360
$(1-f_0)h_{ec}$ (W m^{-2} °C^{-1})	17	15	38	33	29	22
$f_0 h_{Br}$ (W m^{-2} °C^{-1})	9	30	9	34	11	36
$h_{t,cal}$ (W m^{-2} °C^{-1})	362	614	223	346	271	418
relative deviation (%)	7	4	5	8	3	3

† Numerical identified value of K.

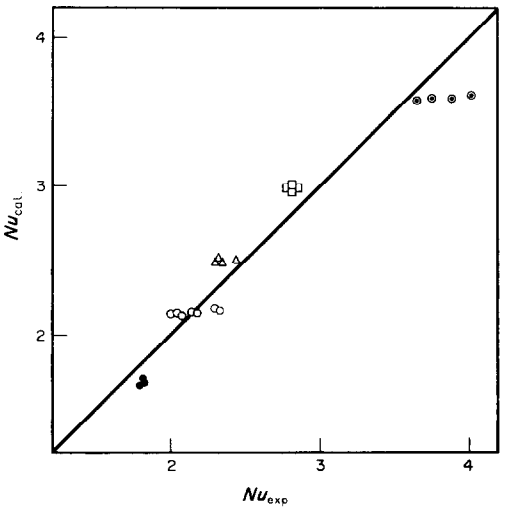

FIG. 10. Comparison of measured and correlated data for the correlation: $Nu = 1.14 Ar^{0.12} N^{-0.14}$.

that the convective component is smaller than the bubble radiative contribution for all particle diameters.

Although calculated and measured data are in good agreement, the validity of the emulsion contribution model [1] is limited to the overall component prediction because the diffusion approximation is not applicable near boundaries. Results of the numerical study show that the calculated radiative contribution depends on the gas film thickness. This observation is consistent with the conclusion of Kolar *et al.* [8] related to the alternate slab model.

As a consequence we do not propose values for the radiative contribution h_{er}.

For engineering design purposes it is useful to dispose of predictive correlations. The whole experimental results are correlated by the following expression:

$$Nu = 1.14 Ar^{0.12} N^{-0.14}, \quad 10^2 < Ar < 10^4, \ 0.4 < N < 10. \quad (31)$$

The mean and maximum differences between calculated and measured Nusselt numbers are 6 and 14%, respectively, as illustrated on Fig. 10.

CONCLUSION

This paper is devoted to the study of the combined heat transfer between a wall and a fluidized bed. Both theoretical and experimental results are presented and compared. The emulsion and bubble phase model contribution are based on heat transfer analysis in semi-transparent media including absorption and scattering. For the bubble phase contribution, the general situation of absorbent gases including particulate is analysed. It is shown that the gas composition—soot in combustors, for example—can double the heat transfer. In the emulsion, the radiative contribution is related to the conduction-to-radiation interaction parameter N. Radiant heat transfer becomes the more important for N values smaller than 5. Mean values of the overall heat transfer coefficient are measured with a two-dimensional 0.25 m^2 column for bed temperatures ranging from 500 to 900°C. The main conclusions of the experimental study are:

(1) A non-linear relation exists between the heat transfer coefficient and the bed temperature for alumina particles whereas it is linear for silicon carbide beds: 60 and 40% increases are observed when the temperature rises from 500 to 900°C.

(2) The radiative contribution becomes significant at temperatures higher than 700°C. It increases with particle diameter.

The comparison between theoretical and experimental results points out that:

(1) At 900°C, the bubble radiative contribution is significant: it ranges between 5 and 9% for our experimental conditions.

(2) The dependence of h on T_b is well correlated to the value of N, conduction-to-radiation parameter. As a consequence, the conductive and radiative emulsion contributions are not independent if $N < 5$.

(3) A good agreement exists between the predicted

and the measured heat transfer coefficients. This permits mean values for extinction coefficients to be proposed for: an alumina bed, 500–1000 m^{-1} and a silicon carbide bed, 5000 m^{-1}, in the temperature range 500–900°C.

Acknowledgement—This work was supported in part by the CNRS-PIRSEM under Grant No. 2034.

REFERENCES

1. G. Flamant et G. Arnaud, Analyse et modélisation du transfert de chaleur entre une paroi et un lit fluidisé à haute température, *Int. J. Heat Mass Transfer* **27,** 1725–1735 (1984).
2. A. P. Baskakof and Yu. M. Goldobin, Radiant heat transfer in a gas fluidized boiling bed, *Heat Transfer—Sov. Res.* **2,** 172–179 (1970).
3. J. S. M. Botteril, Y. Teoman and K. R. Yuregir, Temperature effects on the heat transfer behaviour of gas fluidized beds, *A.I.Ch.E. Symp. Ser.* **77,** 330–340 (1981).
4. J. C. Chen and K. L. Chen, Analysis of simultaneous radiative and conductive heat transfer in fluidized beds, *Chem. Engng Commun.* **9,** 255–271 (1981).
5. A. I. Il'chenko, V. S. Pikashov and K. E. Makhorin, Study of radiative heat transfer in fluidized bed, *J. Engng Phys.* **14,** 602–608 (1968).
6. J. S. M. Botterill and C. J. Sealey, Radiative heat transfer between a gas fluidized bed and an exchange surface, *Br. Chem. Engng* **15,** 1167–1168 (1970).
7. L. J. Jolley, Heat transfer in beds of fluidized solids, *Fuel* **28,** 114–115 (1949).
8. A. K. Kolar, N. S. Grewal and S. C. Saxena, Investigation of radiative contribution in a high temperature fluidized bed using alternate-slag model, *Int. J. Heat Mass Transfer* **22,** 1695–1703 (1979).
9. O. M. Panov, A. P. Baskakov, Yu. M. Goldobin, N. F. Filippovski and Yu. S. Mazur, Experimental investigation of the radiant and conductive–convective component of external heat exchange in a high temperature fluidized bed, *J. Engng Phys.* **36,** 275–279 (1979).
10. R. H. Thring, Fluidized bed combustion for Stirling engine, *Int. J. Heat Mass Transfer* **20,** 911–918 (1977).
11. V. N. Vedamurthy and V. M. K. Sastri, An analysis of the conductive and radiative heat transfer to the walls of fluidized bed combustors, *Int. J. Heat Mass Transfer* **7,** 1–9 (1974).
12. S. T. Wright, The combustion of coal in fluidized beds, XXXVI Int. Cong. Chem. Ind., Bruxelles, Vol. 1, pp. 627–634 (1966).
13. K. Yoshida, T. Veno and D. Kunii, Mechanism of bed wall heat transfer in a fluidized bed at high temperatures, *Chem. Engng Sci.* **29,** 77–82 (1974).
14. J. Szekely and R. J. Fisher, Bed to wall radiation heat transfer in a gas–solid fluidized bed, *Chem. Engng* **24,** 833–849 (1969).
15. V. N. Kharchenko and K. E. Makhorin, The rate of heat transfer between a fluidized bed and immersed body at high temperatures, *Inst. Chem. Engng* **4,** 650–654 (1964).
16. R. Vadivel and V. N. Vedamurthy, An investigation of the influence of bed parameters of the local radiative and total heat transfer coefficient around an embedded horizontal tube in fluidized bed combustors, *Proc. 6th Int. Conf. on Fluid Bed Combustion*, Atlanta, 9–11 April, pp. 1159–1172. DOE (1980).
17. T. F. Ozkaynak, J. C. Chen and T. R. Frankenfield, An experimental investigation of radiation heat transfer in a high temperature fluidized bed, *Fluidization, Proc. 4th Int. Conf. on Fluidization*, Kashikojima, Japan, 29 May–3 June 1983 (Edited by D. Kunii and R. Toei), pp. 371–378. Engineering Foundation (1984).
18. D. Kunii and O. Levenspiel, *Fluidization Engineering*. Wiley, New York (1969).
19. R. Siegel and J. R. Howell, *Thermal Radiation Heat Transfer*. McGraw-Hill, New York (1972).
20. H. C. Hottel and A. F. Sarofim, *Radiative Transfer*. McGraw-Hill, New York (1967).
21. R. O. Skocypec and R. O. Buckius, Total hemispherical emittances for CO_2 or H_2O including particulate scattering, *Int. J. Heat Mass Transfer* **27,** 1–13 (1984).
22. M. Q. Brewster and C. L. Tien, Radiative transfer in packed fluidized beds: dependent versus independent scattering, *J. Heat Transfer* **104,** 573–579 (1982).
23. P. Joulain et J. M. Souil, Emission, absorption des produits de pyrolyse et de combustion dans les incendies, Rencontre SFT, Ville D'Avray, 6–8 Mai (1980).
24. G. Grehan and G. Gouesbet, Mie theory calculations, new progress with emphasis on particle sizing, *Appl. Optics* **8**(20), 3489–3493 (1979).
25. M. Abdelrahman, P. Fumeaux and P. Suter, Study of solid–gas suspensions used for direct absorption of concentrated solar radiation, *Solar Energy* **22,** 45–48 (1979).
26. G. Flamant, Transferts de chaleur couplés dans les lits fluidisés à haute température. Application à la conversion thermique de l'énergie solaire, Thèse de docteur Es-Sciences No. 93, Institut National Polytechnique de Toulouse, 4 mars (1985).
27. M. Granier, Etude du transfert de chaleur entre une couche fluidisée bidimensionnelle et une paroi, Thèse D.I., Institut National Polytechnique de Toulouse (1978).
28. J. S. M. Botterill and A. O. O. Denloye, Gas convective heat transfer to packed and fluidized bed, *A.I.Ch.E. Symp. Ser.* **74**(176), 194–202 (1978).
29. G. Flamant, Theoretical and experimental study of radiant heat transfer in a solar fluidized bed receiver, *A.I.Ch.E. Jl* **28,** 529–535 (1982).

TRANSFERTS DE CHALEUR COUPLES ENTRE UN LIT FLUIDISE ET UNE PAROI. CONTRIBUTIONS DES PHASES BULLE ET EMULSION A HAUTE TEMPERATURE

Résumé—Cet article présente une étude théorique et expérimentale des transferts de chaleur couplés entre une paroi et un lit fluidisé. Les contributions de la phase émulsion et de la phase bulle sont modélisées en faisant l'hypothèse des milieux gris semi-transparents. En ce qui concerne la phase bulle la présence de particules dans le gaz est envisagée. Les essais ont été effectuées avec une colonne bidimensionnelle pour une température moyenne du lit variant de 500 à 900°C. Les conclusions essentielles de ce travail sont (i) l'augmentation de h avec la température n'est pas linéaire lorsque le paramètre d'intéraction conduction-rayonnement, N, est inférieur à 5. Dans ce cas les contributions conductive et radiative de la phase émulsion ne sont pas indépendantes; (ii) la contribution du rayonnement dans la phase dense devient significative au dessus de 700°C; (iii) a 900°C, la contribution radiative de la phase bulle ne peut être négligée.

GEMISCHTE WÄRMEÜBERTRAGUNG VON EINER WAND AN EIN FLIESSBETT—BLASEN- UND EMULSIONSBEITRÄGE BEI HOHEN TEMPERATUREN

Zusammenfassung—Es wird eine theoretische und experimentelle Untersuchung der gemischten Wärmeübertragung von einer Wand an ein Fließbett vorgestellt. Für Blasen- und Emulsionsbeiträge wird ein Modell erstellt, wobei beide Phasen als halbdurchlässige graue Medien betrachtet werden. Für eine strahlende Komponente der Blasen-Phase wird die allgemeine Situation absorbierender, partikelbeladener Gase beschrieben. Es wurden Versuche mit einer 2D-Fließbett-Säule im Temperaturbereich von 500–900°C durchgeführt. Die experimentellen und theoretischen Ergebnisse zeigen, daß (1) eine nichtlineare Beziehung zwischen h und T_b besteht, wenn der Wärmeleitungs-Wärmestrahlungs-Parameter (N) kleiner als 5 ist, was bedeutet, daß Strahlungs- und Wärmeleitungsbeiträge nicht unabhängig voneinander sind, daß (2) die Strahlungsbeiträge der dichten Phase bei Temperaturen oberhalb 700°C bedeutsam werden, und daß (3) bei Temperaturen von 900°C die Strahlungs-Komponente der Blasen-Phase nicht vernachlässigt werden kann.

СЛОЖНЫЙ ТЕПЛООБМЕН МЕЖДУ СТЕНКОЙ И ПСЕВДООЖИЖЕННЫМ СЛОЕМ. ВКЛАД ПУЗЫРЕЙ И ЭМУЛЬСИИ ПРИ ВЫСОКОЙ ТЕМПЕРАТУРЕ

Аннотация—Проводится теоретическое и экспериментальное исследование сложного теплообмена между стенкой и псевдоожиженным слоем. Анализируется вклад пузырей и эмульсии в общий теплообмен в предположении, что обе фазы являются полупрозрачными серыми средами. Используется общий подход—поглощение излучения запыленными газами—для оценки радиационной составляющей пузырьковой фазы. Опыты проводились с двумерным псевдоожиженным слоем при температуре от 500 до 900°C. Экспериментальные и теоретические результаты показали, что (i) между высотой h и температурой T_b существует нелинейная зависимость, если параметр теплопроводность-излучение (N) меньше 5, что указывает на взаимозависимость вкладов излучения и теплопроводности; (ii) вклад излучения плотной фазы становится существенным при температуре выше 700°C; (iii) при 900°C радиационной составляющей пузырьковой фазы пренебрегать нельзя.